

Superfluidity and Chaos in low dimensional circuits

Geva Arwas¹, Amichay Vardi², Doron Cohen¹

¹*Department of Physics, Ben-Gurion University of the Negev, Beer-Sheva, Israel*

²*Department of Chemistry, Ben-Gurion University of the Negev, Beer-Sheva, Israel*

We show that the standard Landau and Bogoliubov superfluidity criteria fail in low-dimensional circuits. Proper determination of the superfluidity regime-diagram must account for the crucial role of chaos, an ingredient missing from the conventional stability analysis. Accordingly, we find novel types of superfluidity, associated with irregular or chaotic or breathing vortex states.

The hallmark of superfluidity is the appearance of a quantized metastable circulating current. Consider a unidirectional flow of particles in a ring. At first it appears that any amount of scattering will randomize the velocity, as in the Drude model, and eventually the ergodic steady state will be characterized by a vanishingly small fluctuating current. However, Landau and followers have shown that this is not always the case [1–5]. If elementary excitations (e.g. phonons) have higher velocity than that of the flow, simple kinematic considerations imply metastability: the energy of the motion cannot dissipate into phonons. On the other hand if this *Landau criterion* is violated the circulating current can decay.

Metastability.— The Landau criterion associates superfluidity with *spectral stability*. The metastability of a circulating flow is determined by checking for accessible elementary excitations (phonons, rotons) connecting the initial state to the quasi-continuum of other states with the same energy [a]. In low dimensional rings superfluidity can persist even if spectral stability is lost [6–10], because *dynamical stability* can still be maintained (see also [11, 12]). But even if dynamical stability is lost, and all regions of the energy-shell are inter-connected, still it does not mean that traffic is allowed between them. Kolmogorov-Arnold-Moser (KAM) surfaces might effectively block completely the passage between different phase-space regions. More generally, remnants of integrable structures may allow only a slow percolation-like penetration process, namely Arnold diffusion. These observations suggest a new paradigm of metastability as discussed below.

Low dimensional circuits.— Integrable (non-chaotic) 1D rings have been extensively studied as models for superfluid circuits [13–20]. However, dimensionality can be further reduced by considering discrete systems of M Bosonic sites. Translational invariance is lost, resulting in the predominance of chaos at low M . Due to number conservation, an M -site model has effectively $d = M - 1$ degrees of freedom. Intensive studies have focused on the Bosonic Josephson Junction ($M=2$ hence $d=1$), which is again an integrable system.

The recent experimental realization of confining potentials with toroidal shapes and tunable weak links [21–23] has opened a new arena of studying superfluidity in low dimensional rings. Of particular notice is the experi-

ment of [15], where a discrete ring has been realized. We are thus motivated to study few-site Bose-Hubbard rings where $M > 2$. In these small discrete circuits the chaos perspective becomes essential for the analysis. The minimal model of interest is the trimer [24–36] which has both non-trivial topology and mixed chaotic phase-space.

The traditional view.— An M site Bosonic system is formally equivalent to a set of coupled oscillators. From a phase-space perspective, the traditional criteria associate stability with the existence of stationary *stable fixed points*. Accordingly, Bogoliubov de Gennes (BdG) linear-stability-analysis is assumed sufficient for determination of the regime where superfluidity is anticipated.

Beyond the traditional view.— The mixed classical phase-space of low dimensional circuits implies three potential aspects in which the traditional stability paradigm is challenged: **(i)** Dynamical instability of a vortex state does not necessarily mean that superfluidity is diminished, because its collapse may be topologically arrested by KAM structures; **(ii)** Linear BdG stability of a vortex state does not always imply actual stability, because Arnold diffusion can provide detour paths out of seemingly elliptical regions; **(iii)** Due to the quantum uncertainty width of a vortex-state, stability is required within a Plank cell around the fixed-point.

The result of these three observations is a novel phase-diagram for the regimes of superfluidity, quite distinct from the one that would be obtained using standard criteria. Considering that the effective number of freedoms is $d = M - 1$ and that Arnold diffusion can only take place when $d > 2$, there should be a dramatic difference between trimers ($M = 3$) and larger rings ($M > 3$): For the trimer, item (i) implies that superfluidity can persist even if the motion becomes *chaotic*; For larger rings, item (ii) implies that BdG (linear) dynamical stability is not a sufficient condition; while item (iii) implies that global analysis of phase-space topography is essential. In the extreme limit of $M \rightarrow \infty$ one should remember that the dynamics become integrable due to rotational symmetry. Below we demonstrate how the above ideas affect the regime diagram of a few site ring. For the trimer ($M = 3$) superfluidity manifests itself beyond the regime of dynamical stability, while for $M > 3$ we find a much more intricate situation.

Model.— Consider N Bosons in a rotating M site ring

system. For theoretical analysis it is more convenient to transform into the rotating frame where the potential is time-independent. In this frame we have Coriolis force, which is formally like having a magnetic flux Φ through the ring (note other options for experimental realization that are mentioned in the concluding paragraphs). Accordingly the system is described by the Bose-Hubbard Hamiltonian [37, 38]

$$\mathcal{H} = \sum_{j=1}^M \left[\frac{U}{2} a_j^\dagger a_j^\dagger a_j a_j - \frac{K}{2} \left(e^{i(\Phi/M)} a_{j+1}^\dagger a_j + \text{h.c.} \right) \right]. \quad (1)$$

Here $j \bmod(M)$ labels the sites of the ring, a_i and a_i^\dagger are destruction and creation operators. K is the hopping frequency, and U is the on-site interaction. The phase Φ is proportional to the rotation frequency of the device. Without loss of generality $\Phi \in [0, \pi]$, and $K > 0$, and $U > 0$. Negative U is the same as positive U with a flipped energy landscape ($\mathcal{H} \mapsto -\mathcal{H}$). Negative K is the same as positive K with $\Phi \mapsto \Phi + \pi$ for odd M . Negative Φ is related to positive Φ by time reversal. The Hamiltonian \mathcal{H} commutes with the total particle number $\mathcal{N} = \sum_i a_i^\dagger a_i$, hence the operator \mathcal{N} is a constant of motion.

In a semi-classical context one defines phase-space action-angle coordinates as follows:

$$a_j = \sqrt{n_j} e^{i\varphi_j} \quad (2)$$

$$z = (\varphi_1, \dots, \varphi_M, \mathbf{n}_1, \dots, \mathbf{n}_M) \quad (3)$$

The Hamiltonian (1) is then expressed as $\mathcal{H} = H(z)$, and the dynamics is generated by $\dot{z} = \mathbb{J} \partial H$. The notation ∂_ν stands for derivative with respect to z_ν , and

$$\mathbb{J} = \begin{pmatrix} 0 & \mathbb{I} \\ -\mathbb{I} & 0 \end{pmatrix} \quad (4)$$

In the classical equation of motion, after standard rescaling of the variables, there are only two dimensionless parameters: one is the dimensionless interaction

$$u = NU/K \quad (5)$$

and the other is the phase Φ . Note that the re-scaling of the canonical variables implies that \mathbf{n} is replaced by \mathbf{n}/N . Hence upon quantization φ and \mathbf{n} are conjugate with dimensionless Planck constant $\hbar = 1/N$.

Regime diagram.— In Fig.1 and Fig.2 we plot the numerically determined (Φ, u) regime diagram for the superfluidity of rings with $M = 3, 4, 5$ sites. Image colors depict $I = \langle (-\partial \mathcal{H} / \partial \Phi) \rangle$ for the eigenstate that carries maximal current. The solid line indicates the spectral stability border and the dashed lines indicates the dynamical stability borders as determined from the BdG analysis (see below). The regime diagrams do not agree with the traditional analysis: For the $M = 3$ ring superfluidity persists beyond the border of dynamical stability,

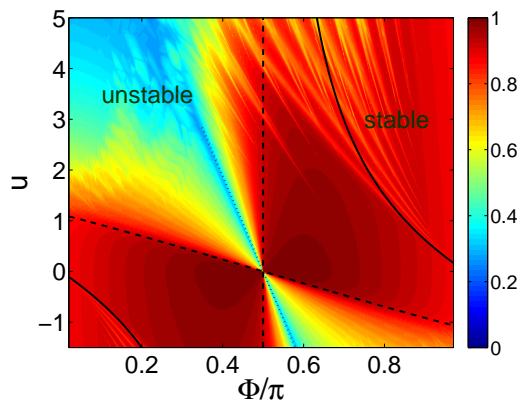


FIG. 1: Regime diagram for the meta-stability of the intermediate vortex state of a Bose-Hubbard trimer with $N=37$ particles. The model parameters are (Φ, u) . The I of the state that carries maximal current is imaged at the background. The solid line indicates the spectral stability border. The dashed lines indicate the dynamical stability borders. The dotted line indicates the “swap” transition (see SM). For clarity we also include a negative u region which is in fact a duplication of the upper sheet.

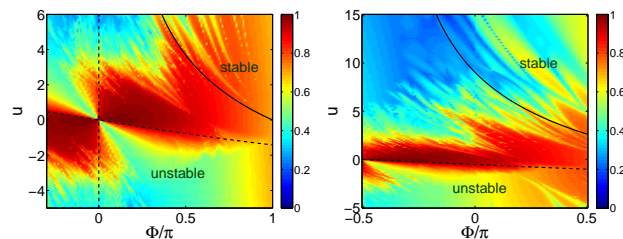


FIG. 2: Regime diagram for an $M=4$ ring with $N=16$ particles (left), and for an $M=5$ ring with $N=11$ particles (right). The image and the lines are defined as in Fig.1. Here the dynamical stability condition is not sufficient to ensure superfluidity due to “Arnold diffusion”. As u becomes larger this non-linear leakage effect is enhanced, the stability of the vortex state is deteriorated, and the current is diminished.

while for $M > 3$ the dynamical stability condition is not sufficient.

In principle, stability should also be verified with respect to added disorder W (random on-site energies). Some reflection leads to the realization that the meta-stability of the vortex fixed-point (see below) is maintained as long as $W < U$. This means that superfluidity requires *finite* strength of interaction. To be sure, we have verified that the numerically determined regime diagrams are not affected by adding weak disorder.

Vortex states.— The stationary orbitals of a single particle in a clean ring are the momentum states with wavenumber $k = (2\pi/M)m$, where m is an integer modulo M . Coherent vortex states have N particles *condensed* into the same momentum orbital. From a semi-

classical perspective, a coherent state is represented by a minimal-Gaussian-like phase-space distributions.

Stability analysis.— A stable stationary fixed point of the classical Hamiltonian can support a coherent eigenstate. Here we focus on *vortex states* (there are also solitons [24, 25, 27–29, 31, 33] and modulated solutions [39], see SM). A stationary fixed point is the solution of the equation $\partial H = 0$. In the vicinity of a fixed point the equation of motion takes the form $\dot{z} = \mathbb{J}\mathcal{A}z$, where the Hessian matrix is

$$\mathcal{A}_{\nu,\mu} = \partial_\nu \partial_\mu H \quad (6)$$

A fixed-point is *spectrally* stable if it resides at a local minimum or maximum of $H(z)$. Its dynamical stability is determined by the roots of the characteristic equation $\det(\lambda - \mathbb{J}\mathcal{A}) = 0$. (The zero eigenvalues that are associated with the cyclic degree of freedom \mathcal{N} should be excluded, so effectively we deal with $2d \times 2d$ matrix where $d = M-1$). At the spectral stability border, where the fixed-point becomes a saddle, we have $\det(\mathcal{A}) = \det(\mathbb{J}\mathcal{A}) = 0$.

Upon quantization the eigenvalues λ are identified as the energies of the Bogoliubov excitations. The fixed-point becomes dynamically unstable if the eigenvalues acquire a real part, known as the Lyapunov exponent.

Vortex states correspond to the trivial fixed-points of the Hamiltonian, located along the symmetry axis $n_1 = \dots = n_M = N/M$. The m th vortex state, with $\varphi_i - \varphi_{i-1} = (2\pi/M)m$, corresponds to condensation in the m th momentum orbital. The vortex states have a macroscopically large current:

$$I_m = \left\langle -\frac{\partial \mathcal{H}}{\partial \Phi} \right\rangle_m = \frac{N}{M} K \sin \left(\frac{1}{M} (2\pi m - \Phi) \right) \quad (7)$$

The BdG stability analysis of the vortex states is quite straightforward (see SM) and leads to the solid and dashed lines of Fig.1 and Fig.2. We note that the BdG analysis of the vortex states of $M > 3$ rings leads to similar expressions, because at the vicinity of the symmetry axis the interaction is negligible. As we go away from the symmetry axis the interaction becomes more important, and the value of M becomes significant.

Superfluidity.— Once $\Phi \neq 0$ time reversal is broken and the ground state can carry a “persistent current”. The current goes to zero in the limit $\Phi \rightarrow 0$. Superfluidity is the possibility to have a macroscopically large metastable current for $\Phi \rightarrow 0$. Metastability is achieved thanks to the interaction U . In our ring model superfluidity is feasible if a middle vortex state is stable. Instability of this state implies it would mix with all the other eigenstates residing in the same energy shell, resulting in a micro-canonically small current.

As shown in Fig.1 and Fig.2 the observed superfluidity regimes are not in accordance with the traditional BdG analysis. First of all, irrespective of M , as we go

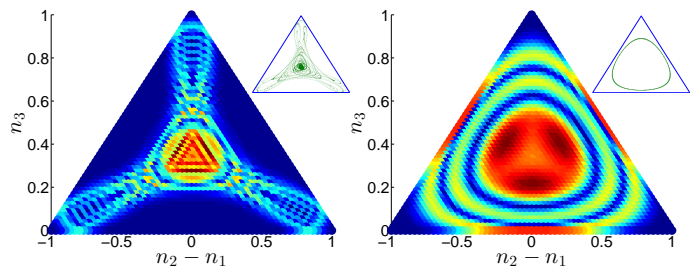


FIG. 3: Wavefunctions of exotic vortex states. Chaotic vortex state (left); and breathing vortex state (right) of an $N=60$ trimer are imaged. The names are related to the underlying classical dynamics (insets) which is chaotic or periodic respectively. The parameters (Φ, u) are $(0.36\pi, 1.3)$ and $(0.05\pi, 1.5)$. Note that a regular vortex (not displayed) would be represented by a simple hump at the central $(n_1=n_2=n_3)$ fixed-point. The occupation axis is scaled ($n \mapsto n/N$).

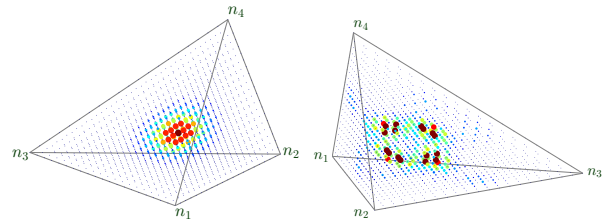


FIG. 4: Wavefunctions of regular vortex state (left) and irregular vortex state (right) of $M=4$ ring with $N=20$ particles. The axes are as in Fig.3 with one extra dimension. The parameters (Φ, u) are $(0.2\pi, 0)$ and $(0.2\pi, 3)$ respectively. Note that a regular vortex is represented by a simple hump at the central $(n_1=n_2=n_3=n_4)$ fixed-point, whereas an irregular vortex has a richer structure that reflects the fragmented phase-space structure.

higher in u , superfluidity is diminished even in the spectrally stable region. This is conspicuous for low N , as in Fig.2b, and can be explained as the consequence of having a finite uncertainty width. Namely, as u is increased the radius of the stability island (if exists) becomes smaller, until eventually it cannot support a stable vortex state. Equivalently, as N becomes smaller the uncertainty width of a vortex state becomes larger, until it ‘spills’ out of the stability island. This type of reasoning resembles the semiclassical view of the Mott transition (see SM). Taking a closer look at the regime diagrams one observes that the above “quantum fluctuations” perspective is not enough in order to explain the observed differences. We therefore turn to provide a more detailed phase-space picture.

The $M = 3$ ring.— We observe macroscopically large currents beyond the expected region. This has been noted in [36] without explanation. In particular we see that superfluidity survives in the limit $\Phi \rightarrow 0$, contrary to the expectation [40] that is based on the traditional

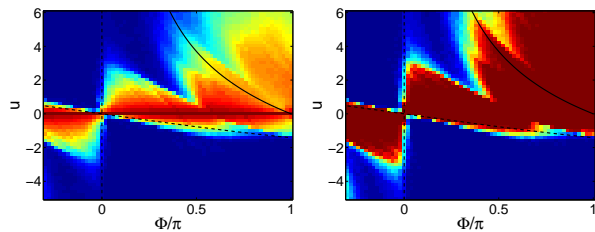


FIG. 5: Semiclassical reproduction of the regime phase diagram. We use a very simple numerical procedure to establish the semiclassical interpretation of Fig.2, and its N dependence. Given (Φ, u) we launch a Gaussian cloud of trajectories that have an uncertainty width that corresponds to N . The fraction of trajectories (blue $\sim 100\%$ to red $\sim 0\%$) that escape is used as a measure for stability (see text for details). Results are displayed for clouds that have uncertainty width $\Delta\varphi \sim \pi/2$ (left) and $\Delta\varphi \sim \pi/4$ (right). The lines are the stability borders of Fig.2a.

stability argument.

We can plot the wavefunction $|\Psi(r)|^2 = |\langle r|E_\alpha\rangle|^2$ of an eigenstate that support superfluidity. Here the standard basis coordinates are $r_{\parallel} = (n_2 - n_1)/N$ and $r_{\perp} = n_3/N$. The wavefunction of a standard *regular* vortex is merely a hump at the symmetry point $n_1 = n_2 = n_3 = N/3$. In Fig.3 we display examples for the wavefunctions of non-standard vortex states: a *chaotic* vortex state, and a *breathing* vortex state. The terms "chaotic" and "breathing" is related to the underlying classical dynamics [options (ii) and (iii) below].

Launching trajectories at the vicinity of the vortex fixed-point we encounter the following possibilities: **(i)** the trajectories are locked in the vicinity of the vortex fixed point; **(ii)** the trajectories are quasi-periodic in phase-space; **(iii)** the trajectories are chaotic but unidirectional. Poincare sections of the trajectories (see SM) reveal that a regular vortex state is supported by a regular island around the fixed point (case i); a breathing vortex is supported by a secondary island that has been created via bifurcation (case ii); while a chaotic vortex state is supported by a 'chaotic pond' of clockwise motion that does not mix with the anti-clockwise motion (case iii). Consequently the motion may become chaotic, but stay unidirectional, and superfluidity persists contrary to the common expectation.

The $M > 3$ rings.— Considering a no-rotating device, the traditional stability argument [40] implies marginally stable superfluidity for an $M = 4$ device, and stability if u is large enough for an $M > 4$ device. These observations are implied by the stability borders that are plotted in Fig.2. Looking on the numerically determined current one observes that superfluidity can persist slightly beyond the dynamical stability border. But much more conspicuous is the diminishing of superfluidity within a large region where the BdG analysis predicts dynamical sta-

bility. We find (see below) that the latter effect is related to Arnold diffusion. Namely, if $d > 2$, the d dimensional KAM tori in phase space are not effective in blocking the transport on the $2d-1$ energy shell. As u becomes larger this non-linear leakage effect is enhanced, stability of the motion is deteriorated, and the current is diminished.

At this point it might be helpful to distinguish between *strict* dynamical stability and *linear* dynamical stability. For $M > 3$ the latter does not imply the former. As we go up in u the chaos becomes predominant, and consequently spectral stability rather than dynamical stability becomes the relevant criterion. It follows from this distinction that for $M > 3$ one has to distinguish between regular and irregular vortex states. This distinction is demonstrated in Fig.4. A regular vortex is represented by a simple hump at the central ($n_i = N/M$) fixed-point, whereas an irregular vortex has a richer structure that reflects the underlying fragmented phase-space structure.

In order to verify the above semiclassical reasoning, we try in Fig.5 to reconstruct the quantum regime-diagram via classical simulations. This reconstruction provides a qualitative proof for the semiclassical reasoning, and furthermore demonstrates the N dependence of the the superfluidity regime diagram. Namely, we launch a Gaussian cloud of trajectories that have an uncertainty width that corresponds to N . The fraction of trajectories that escape is used as a measure for the stability. The practical criterion for escape is having the average current $I(t)$ getting below some threshold I_∞ within some time t_∞ . In principle t_∞ should be the Heisenberg time (proportional to N^d), and I_∞ can be (say) half I_m . In practice the result is not sensitive to these thresholds.

Conclusions.— We have highlighted a novel type of superfluidity that is supported by irregular or chaotic or breathing vortex states. Such states are supported by fragmented regions in phase-space ($M > 3$), or by chaotic ponds ($M = 3$), or by periodic-orbits respectively, hence they are missed by the traditional BdG analysis. Furthermore we have highlighted the limitations of the *linear* stability analysis for high dimensional chaos ($M > 3$).

In a larger perspective we emphasize that the role of chaos should be recognized in the analysis of superfluidity. Furthermore we believe that a global understanding of the mixed phase-space structure is essential in order to analyse dynamical processes such as phase-slips [6, 22, 23, 41]. Accordingly it is important to identify what type of meta-stability is responsible for the superfluidity.

The specific ring geometry of Eq. (1) has been experimentally realized [15] by forming an optical lattice [42, 43]. A phase Φ is implied by introducing a spatially-adiabatic variation of the atomic magnetic dipole orientation [42]. Optionally one can use rotating laser fields as demonstrated for a toroidal shaped trap [23], or introduce gauge field as in [44], see [45].

Acknowledgements.— This research has been supported by the Israel Science Foundation (grant Nos. 346/11 and 29/11) and by the United States-Israel Binational Science Foundation (BSF).

-
- [1] L.D. Landau, *J. Phys. (Moscow)* **5**, 71 (1941).
- [2] V. Hakim, *Phys. Rev. E* **55**, 2835 (1997). [link]
- [3] M. Albert, T. Paul, N. Pavloff, P. Leboeuf, *Phys. Rev. A* **82**, 011602(R) (2010). [link]
- [4] R.P. Feynman, *Statistical Mechanics: A Set of Lectures* (Westview Press, Boulder, CO, 1998).
- [5] C. Raman, M. Kohl, R. Onofrio, D.S. Durfee, C.E. Kulewicz, Z. Hadzibabic, W. Ketterle, *Phys. Rev. Lett.* **83**, 2502 (1999). [link]
- [6] A. Polkovnikov, E. Altman, E. Demler, B. Halperin, M.D. Lukin, *Phys. Rev. A* **71**, 063613 (2005) [link]
- [7] B. Wu and Q. Niu, *New J. Phys.* **5**, 104 (2003). [link]
- [8] A. Smerzi, A. Trombettoni, P.G. Kevrekidis, and A.R. Bishop, *Phys. Rev. Lett.* **89**, 170402 (2002). [link]
- [9] F.S. Cataliotti, L. Fallani, F. Ferlaino, C. Fort, P. Maddaloni, M. Inguscio, *New J. Phys.* **5**, 71 (2003). [link]
- [10] L. De Sarlo, L. Fallani, J.E. Lye, M. Modugno, R. Saers, C. Fort, and M. Inguscio, *Phys. Rev. A* **72**, 013603 (2005). [link]
- [11] A.R. Kolovsky, H.J. Korsch, E.M. Graefe, *Phys. Rev. A* **80**, 023617 (2009). [link]
- [12] J.R. Anglin, *Phys. Rev. A* **67**, 051601 (2003). [link]
- [13] R. Kanamoto, H. Saito, M. Ueda, *Phys. Rev. A* **68**, 043619 (2003), [link]
- [14] A.Yu. Cherny, J.-S. Caux, J. Brand, *Frontiers of Physics* **7**, 54 (2012). [link]
- [15] L. Amico, D. Aghamalyan, F. Auksztol, H. Crepaz, R. Dumke, L.C. Kwek, *Sci. Rep.* **4**, 4298 (2014). [link]
- [16] A.M. Rey, K. Burnett, I.I. Satija, C.W. Clark, *Phys. Rev. A* **75**, 063616 (2007). [link]
- [17] D.W. Hallwood, K. Burnett, J. Dunningham, *New J. Phys.* **8**, 180 (2006). [link]
- [18] A. Nunnenkamp, A.M. Rey, K. Burnett, *Phys. Rev. A* **84**, 053604 (2011). [link]
- [19] D. W. Hallwood, T. Ernst, J. Brand, Robust mesoscopic superposition of strongly correlated ultracold atoms. *Phys. Rev. A* **82**, 063623 (2010). [link]
- [20] M. Cominotti, D. Rossini, M. Rizzi, F. Hekking, A. Minguzzi, *Phys. Rev. Lett.* **113**, 025301 (2014). [link]
- [21] C. Ryu, M. F. Andersen, P. Clade, V. Natarajan, K. Helmerson, W. D. Phillips, *Phys. Rev. Lett.* **99**, 260401 (2007). [link]
- [22] S. Moulder, S. Beattie, R. P. Smith, N. Tammuz, Z. Hadzibabic, *Phys. Rev. A* **86**, 013629 (2012). [link]
- [23] K.C. Wright, R.B. Blakestad, C.J. Lobb, W.D. Phillips, G.K. Campbell, *Phys. Rev. Lett.* **110**, 025302 (2013). [link]
- [24] J.C. Eilbeck, P.S. Lomdahl, A.C. Scott, *Physica D* **16** 31838 (1985). [link]
- [25] D. Hennig, H. Gabriel, M.F. Jorgensen, P.L. Christiansen, C.B. Clausen, *Phys. Rev. E* **51**, 2870 (1995). [link]
- [26] S. Flach and V. Fleurov, *J. Phys.: Condens. Matter* **9**, 7039 (1997). [link]
- [27] K. Nemoto, C.A. Holmes, G.J. Milburn, and W.J. Munro, *Phys. Rev. A* **63**, 013604 (2000). [link]
- [28] R. Franzosi, V. Penna, *Phys. Rev. E* **67**, 046227 (2003). [link]
- [29] M. Johansson, *J. Phys. A: Math. Gen.* **37** (2004). [link]
- [30] M. Hiller, T. Kottos, and T. Geisel, *Phys. Rev. A* **73**, 061604(R) (2006). [link]
- [31] T.F. Viscondi, K. Furuya, *J. Phys. A* **44**, 175301 (2011). [link]
- [32] P. Jason, M. Johansson, K. Kirr, Quantum signatures of an oscillatory instability in the Bose-Hubbard trimer. *Phys. Rev. E* **86**, 016214 (2012). [link]
- [33] P. Buonsante, V. Penna, and A. Vezzani, *Phys. Rev. A* **82**, 043615 (2010). [link]
- [34] C. Lee, T. J. Alexander, and Y.S. Kivshar, *Phys. Rev. Lett.* **97**, 180408 (2006). [link]
- [35] A.R. Kolovsky, *Phys. Rev. Lett.* **99**, 020401 (2007). [link]
- [36] G. Arwas, A. Vardi, D. Cohen, *Phys. Rev. A* **89**, 013601 (2014). [link]
- [37] O. Morsch, M. Oberthaler, *Rev. Mod. Phys.* **78**, 179 (2006). [link]
- [38] I. Bloch, J. Dalibard, and W. Zwerger, *Rev. Mod. Phys.* **80**, 885 (2008). [link]
- [39] M. Machholm, A. Nicolin, C.J. Pethick, H. Smith, *Phys. Rev. A* **69**, 043604 (2004). [link]
- [40] P. Ghosh, F. Sols, *Phys. Rev. A* **77**, 033609 (2008) [link]
- [41] D. McKay, M. White, M. Pasienski, B. DeMarco, *Nature* **453**, 76 (2008). [link]
- [42] L. Amico, A. Osterloh, and F. Cataliotti, *Phys. Rev. Lett.* **95**, 063201 (2005). [link]
- [43] K. Henderson, C. Ryu, C. MacCormick, M.G. Boshier, *New J. Phys.* **11** 043030 (2009) [link]
- [44] Y.J. Lin, R.L. Compton, K. Jimenez-Garcia, J.V. Porto, I.B. Spielman, *Nature* **462**, 628632 (2009). [link]
- [45] J. Dalibard, F. Gerbier, G. Juzeliunas, P. Öhberg, *Rev. Mod. Phys.* **83**, 1523 (2011). [link]
- [a] While quantum mechanics allows tunnelling through classically-forbidden regions into the allowed quasi-continuum, this 'phase slip' process [6, 22, 23, 41] is much slower and is therefore ignored in the semi-classical analysis.

SUPPLEMENTARY MATERIAL

Stability analysis.— For pedagogical reason we focus on the trimer, but the generalization to $M > 3$ is straightforward. We focus on the central region of energy space, where the middle vortex state ($m = 1$) is located. The dynamical stability is determined by the characteristic equation $\det(\lambda - \mathbb{J}\mathcal{A}) = 0$. Two trivial eigenvalues $\lambda = 0$ reflect the constant of motion \mathcal{N} , and therefore excluded. The other four eigenvalues are the solution of $\lambda^4 + b\lambda^2 + c = 0$ with

$$c = \sin^2\left(\frac{\Phi}{3} - \frac{\pi}{6}\right) \left[u - \frac{3 - 12\sin^2\left(\frac{\Phi}{3} - \frac{\pi}{6}\right)}{4\sin\left(\frac{\Phi}{3} - \frac{\pi}{6}\right)} \right]^2 \quad (8)$$

$$b = \frac{3}{2} + 3\sin^2\left(\frac{\Phi}{3} - \frac{\pi}{6}\right) + 2u\sin\left(\frac{\Phi}{3} - \frac{\pi}{6}\right) \quad (9)$$

Upon quantizations the λ s can be identified as the energies of the Bogoliubov excitations. A fixed-point is spectrally (meta) stable if it seats at a (local) minimum or maximum of $H(z)$. At the spectral stability border, where the fixed-point becomes a saddle, we have $\det(\mathcal{A}) = \det(\mathbb{J}\mathcal{A}) = 0$, hence the border is determined by $c = 0$, leading to the spectral stability condition

$$u > \frac{3 - 12\sin^2\left(\frac{\Phi}{3} - \frac{\pi}{6}\right)}{4\sin\left(\frac{\Phi}{3} - \frac{\pi}{6}\right)} \quad (10)$$

The fixed-point becomes dynamically unstable if the eigenvalues acquire a real part, which is the so-called Lyapunov exponent. This happen when $b^2 - 4c < 0$, leading to dynamical instability in the region

$$u > \frac{9}{4}\sin\left(\frac{\pi}{6} - \frac{\Phi}{3}\right) \quad \& \quad \Phi < \frac{\pi}{2} \quad (11)$$

In principle for $b^2 - 4c > 0$ the condition $b < 0$ would imply an additional dynamical instability regime. But here $b < 0$ occurs inside the region of $b^2 - 4c < 0$. The stability borders are demonstrated in Fig.1.

Swap scenario.— Inspecting Fig.1 one observes that superfluidity diminishes in the vicinity of the indicated dotted line. It turns out that the swap scenario is originated from a global non-linear resonance. This can be established by inspection of Poincare sections (see below): at the transition two separatrices swap in phase-space. In order to derive the resonance condition we rewrite the Hamiltonian Eq.(1) using:

$$b_0 = \frac{1}{\sqrt{3}}(a_1 + a_2 + a_3), \quad b_{\pm} = \frac{1}{\sqrt{3}}\left(a_1 e^{\pm i \frac{2\pi}{3}} + a_2 e^{\pm i \frac{4\pi}{3}} + a_3\right) \quad (12)$$

This leads to:

$$\mathcal{H} = \omega_0 n_0 + \omega_+ n_+ + \omega_- n_- \quad (13)$$

$$+ \frac{U}{6} [n_0^2 + n_+^2 + n_-^2 + 4(n_0 n_+ + n_0 n_- + n_+ n_-)] \quad (14)$$

$$+ \frac{U}{12} [(b_+^\dagger b_+^\dagger b_- b_0 + b_0^\dagger b_-^\dagger b_+ b_+) + (b_0^\dagger b_0^\dagger b_+ b_- + b_-^\dagger b_+^\dagger b_0 b_0) + (b_-^\dagger b_-^\dagger b_0 b_+ + b_+^\dagger b_0^\dagger b_- b_-)] \quad (15)$$

where $\omega_0 = -K \cos(\Phi/3)$, and $\omega_{\pm} = -K \cos(\pm 2\pi/3 - \Phi/3)$. We consider the subspace of states with $n_0 - n_- = 0$, and keep only the resonant coupling $(b_+^\dagger)^2 b_- b_0$ and its conjugate. Then we define the reaction coordinate is $J_z = (1/4)(2n_+ - N)$, associated ladder operators J_{\pm} , and hooping generator $J_x = (J_+ + J_-)/2$, such that the Hamiltonian takes the form:

$$\mathcal{H} \approx \left(2\omega_+ - \omega_- - \omega_0 - \frac{UN}{6}\right) J_z - U J_z^2 + \frac{U}{3} [(N/4)^2 - J_z^2]^{1/2} J_x + \text{const} \quad (16)$$

The non-linear resonance happens if the first term vanishes, leading to

$$u = 18 \sin\left(\frac{\pi}{6} - \frac{\Phi}{3}\right) \quad (17)$$

In general superfluidity diminishes whenever regions in phase-space are scrambled. The swap scenario is possibly the simplest scenario. Such type of separatrix overlap bifurcation has been once encountered in molecular physics studies [J.F. Svitak , V. Tyng , and M.E. Kellman, J. Phys. Chem. A, 2002, 106 (45)] (but not in chaotic context).

Solitons.— While our main focus is on the stability of vortex states we briefly discuss other fixed points that were of interest in past work. The trimer model without rotation ($\Phi = 0$) has been the subject of intense study [24–35]. In particular it has been noted that the Hamiltonian $H(z)$ has additional non trivial fixed-points away from the symmetry axis. The simplest of which are self-trapped “bright solitons” obtained via bifurcation of a vortex state, in which the particles are localized in a single site. This self-trapping transition happens outside of the interval $-2.25 < u < 0$. Other notable fixed-points correspond to single-depleted-well states in which one site is empty, while the remaining two sites are equally occupied by the particles. For $M > 3$ rings there are off-axis fixed points that support spatially modulated vortex states [39].

The ground state.— The lowest energy fixed-point ($m = 0$ vortex state) is stable for any positive u . However it is located in an island which is surrounded by a chaotic sea. As u is increased the island’s size decreases until at $u > N^2/M$, it becomes smaller than a single Planck cell. At this point it can no longer accommodate a vortex state and one observes a quantum Mott transition. Other studies of rotating ring lattices [15–20] have addressed additional quantum issues, such as the appearance of “cat states”: In the trimer with $\Phi = \pi$ the ground state might be a macroscopic superposition of the degenerate vortex states $m=0$ and $m=1$.

Purity.— Any many-body state can be characterized by its one-body-coherence. The precise definition of the associated “purity” measure S can be found in [36]. Here it is enough to say that $S = 1$ means that all the particle are condensed in a single orbital, while $S < 1$ means that the state is fragmented into $1/S$ orbitals. For ergodic state $1/S \sim M$. It turns out that the non-standard vortex states have high but not perfect purity. See spectra in Fig.7.

Poincare sections.— Starting with the Hamiltonian Eq.(1) written in terms of action-angle variables, the classical dynamics is generated by the equation

$$i \frac{\partial a_i}{\partial t} = \frac{\partial \mathcal{H}}{\partial a_i^*} = u |a_i|^2 a_i - \frac{1}{2} \left[e^{i\Phi/3} a_{i-1} + e^{-i\Phi/3} a_{i+1} \right] \quad (18)$$

with scaled units such that $K = N = 1$. We solve this equation numerically. For plotting of trajectories it is convenient to use the coordinates $(n_1 - n_3, \varphi_1 - \varphi_3)$ and $(n_3 - n_2, \varphi_3 - \varphi_2)$. The section chosen is $n_3 - n_2 = 0$, at the energy of the $m = 1$ vortex, namely,

$$E = \frac{u}{6} - \cos \left(\frac{2\pi}{3} - \frac{\Phi}{3} \right) \quad (19)$$

Given a phase space section point $(n_1 - n_3, \varphi_1 - \varphi_3)$, the equation $H(z) = E$ has either zero or two solutions for the remaining coordinate $\varphi_3 - \varphi_2$. This implies that the Poincare section has two sheets. For presentation purpose we pick the sheet where velocity $\partial_t(n_3 - n_2)$ has a larger value. On this sheet the boundary of the allowed region, is marked by a black line. The current of a generated trajectory is calculated by taking a time average over \mathcal{I} .

Phase-space tomography.— In Fig.7 we plot the spectrum of the trimer Hamiltonian for representative values of (Φ, u) that are indicted in Fig.6. We also plot in each case a Poincare section at the energy of the $m = 1$ vortex fixed-point, for $n_3 - n_2 = 0$. For convenience we use the canonical coordinates $(n_1 - n_3, \varphi_1 - \varphi_3)$ and a scaled particle number $n \mapsto n/N$. Each point in the Poincare section is colored according to the current, averaged over the classical trajectory. Note that the $m = 1$ vortex fixed-point is always located at $(0, 2\pi/3)$. From the quantum spectrum we can easily deduce the phase-space structure at *any other energy*. One can call it “quantum phase-space tomography”. Consider for example Fig.7c. We can easily correlate the largest current states with the red (upper) island; the secondary group of large current states with the yellow (left) island; and the small current states with the green chaotic sea. Additional information can be extracted from the purity of the states. Points in the spectrum are colorcoded from black ($S \sim 1$) to purple ($S \sim 1/M$).

By inspection of Fig.7 we observe the following regimes in the diagram of Fig.1: Regime (S) stands for simple phase-space structure with spectrally stable clockwise (“red”) and anti-clockwise (“blue”) islands that are separated by a forbidden region. In regime (B) we have two regular regions of clockwise motion, and “blue separatrix” that supports anti-clockwise motion. As we go up in u the blue separatrix becomes a chaotic sea. In regime (D) the middle

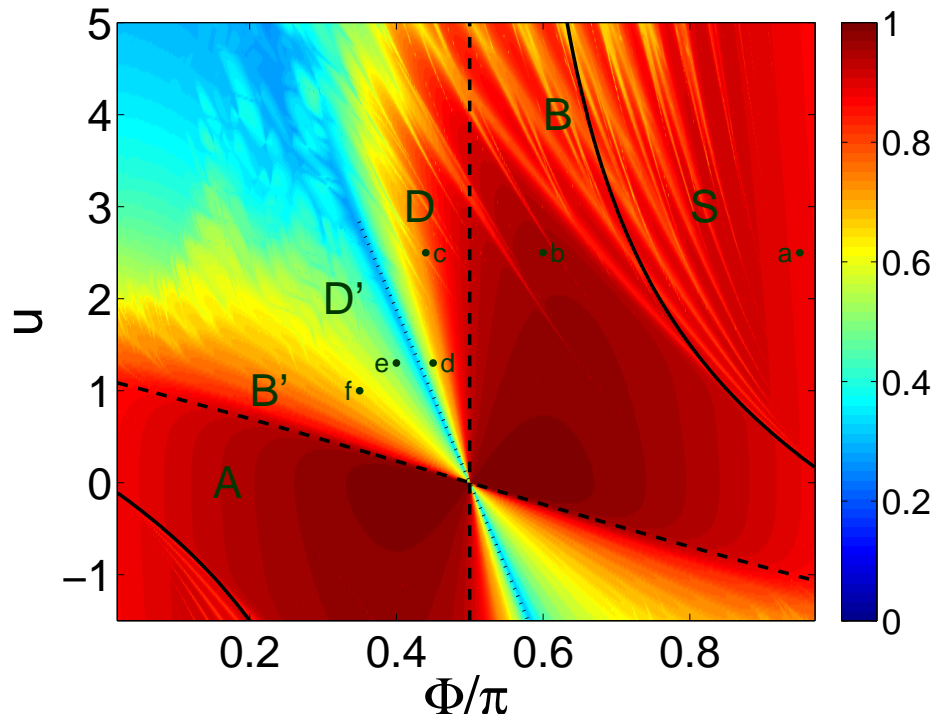


FIG. 6: Same as Fig.1 with extra indications (see text). The dots labeled (a-f) mark (Φ, u) coordinates that are used in Fig.7 to demonstrate the different regimes.

vortex bifurcates, while the other clockwise island remains regular. In regime (D') the “vortex separatrix” swaps with the “blue separatrix”. This swap is clearly demonstrated as we go from Fig.7d to Fig.7e. The border between regimes (D) and (D') is shown as a dotted line in Fig.1, see Eq.(17). Along this line the two separatrices coalesce. Crossing to regime (B') the bifurcation that is responsible to the “blue separatrix” is undone, and eventually we can go back to the (S) regime via a simply-connected (A) regime that has a simple structure with no separatrix.

In region (B) the vortex is not spectrally stable: it is located on a saddle point in phase-space. Nevertheless dynamical stability is maintained. In region (D) the vortex is no longer dynamically stable, and the trajectories at the vicinity of the vortex are chaotic. Still the motion is confined by KAM tori within a “chaotic pond”, and therefore remains uni-directional. In the vicinity of the swap, as we go up in u , the chaotic pond becomes a chaotic sea, and the superfluid current is diminished.

Upon quantization the chaotic pond can support a “chaotic vortex state”, which has been illustrated in Fig.3a. A second class of large current states are supported by stable *periodic-orbits* (POs) that has been bifurcated from the stationary vortex fixed-point, once the latter lost stability. These POs are elliptic fixed-points of the Poincare section, see Fig.7d. Upon quantization the associated islands can support a “breathing vortex state”, see Fig.3b.

Secondary message.— As a secondary message, we would like to emphasize that the gross features of the classical phase-space can be easily extracted from the spectrum of the quantized Hamiltonian. To get the same information via classical analysis would be an extremely heavy task that would require generation of many trajectories in numerous phase space regions, on each possible energy shell, as opposed to our “quantum phase space tomography” which requires a single diagonalization of a finite matrix. If Nature were classical, Quantum Mechanics still would be invented as a valuable tool, just for the purpose of analysing mixed complex dynamics.

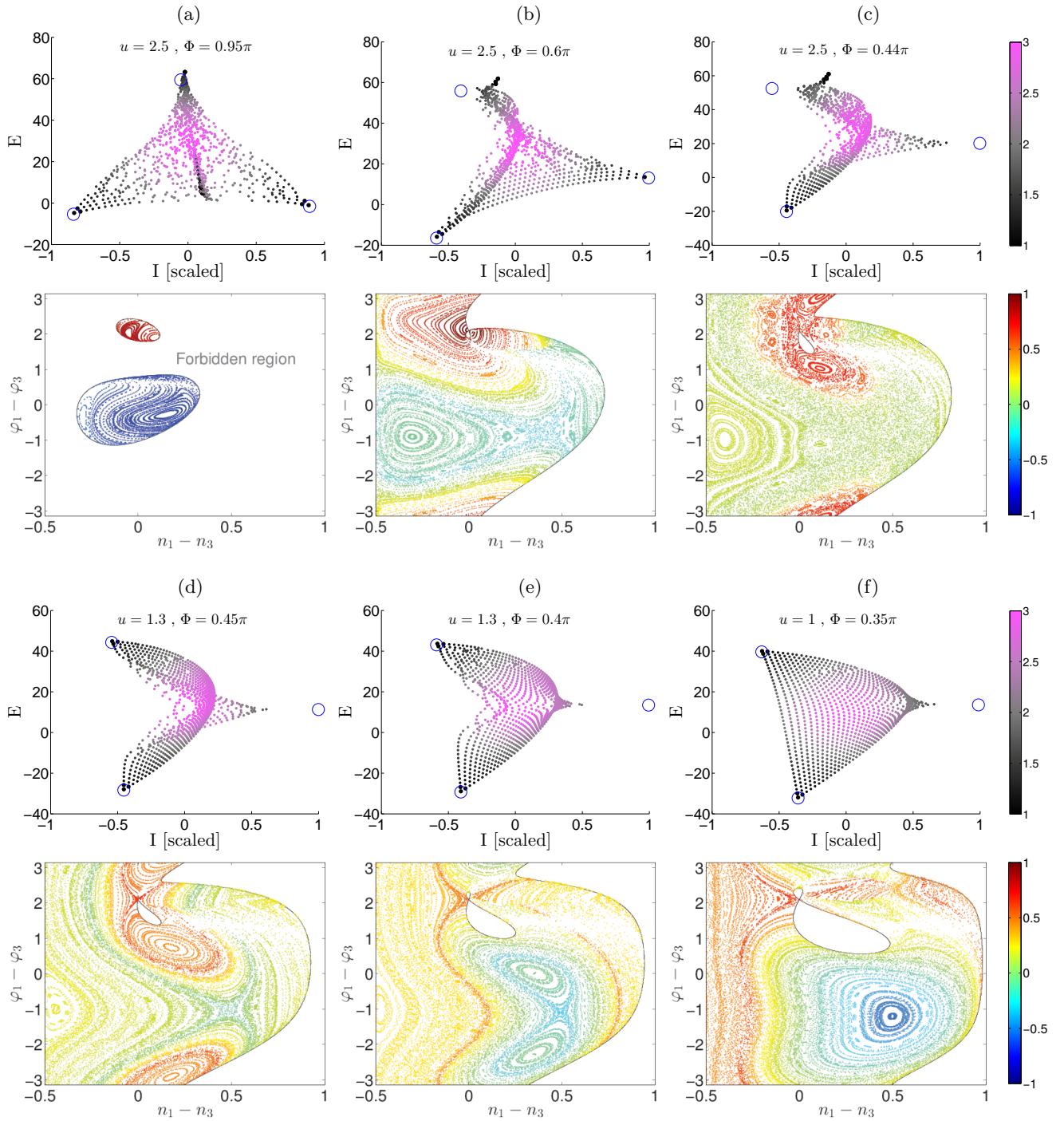


FIG. 7: **Quantum spectrum and phase-space landscape.** Representative quantum spectra of for an $N = 42$ trimer for representative (Φ, u) values. Panels (a-f) are for $(0.95\pi, 2.5)$; $(0.6\pi, 2.5)$; $(0.44\pi, 2.5)$; $(0.45\pi, 1.3)$; $(0.4\pi, 1.3)$; $(0.35\pi, 1)$. Each point represents an eigenstate color-coded by its purity (black $(1/S) \sim 1$ to purple $(1/S) \sim 3$), and positioned according to its energy E_α and its scaled current $I_\alpha/(NK/M)$. In each case an $n_3 - n_2 = 0$ Poincare section at the energy of the $m = 1$ vortex is displayed (with the exception of (a) where it is for a slightly shifted energy, else the red island would shrink into a point). The solid black line marks the borders of the allowed phase-space regions. The color code represents the averaged current for each classical trajectory.